Supporting Information for:

# *Post-passivation of multication perovskite with rubidium butyrate*

*José Carlos Germino,[1,§] Rodrigo Szostak,[1,2,§] Silvia G. Motti,[3] Raphael F. Moral,[1] Paulo E. Marchezi,[1] Heitor S. Seleghini,[1] Luiz G. Bonato,[1] Francineide Lopes de Araújo,[1] Teresa D. Z. Atvars,[1] Laura M. Herz,[3] David Fenning,[4] Anders Hagfeldt[2] and Ana Flávia Nogueira[1,*]*

§ The authors contributed equally to this work

*Corresponding author: anafla@unicamp.br

[1] University of Campinas (UNICAMP), Laboratório de Nanotecnologia e Energia Solar, Chemistry Institute, Campinas, PO Box 6154, 13083-970, Brazil.

[2] Laboratory of Photomolecular Science, Institute of Chemical Sciences and Engineering, École Polytechnique Fédérale de Lausanne, 1015, Lausanne, Switzerland

[3] Department of Physics, University of Oxford, Clarendon Laboratory, Parks Road, Oxford OX1 3PU, United Kingdom.

[4] Department of Nanoengineering, University of California, San Diego, La Jolla, CA 92093, USA.

This supporting information contains experimental details concerning the materials, synthesis of RbBu, preparations of perovskite and surface modification, structural and optical characterization methods, PSCs assembly and characterization method, theoretical calculations, additional characterization data, and supplementary texts 1, 2 and 3.

## Experimental Details

### Materials

Lead iodide ($PbI_2$, 99.99%) and lead bromide ($PbBr_2$, 99.99%) were purchased from TCI America, 9211 N. Harborgate St., Portland, OR 97203, USA. Cesium iodide (CsI, 99.9 %), butyric acid ($BuCO_2H$, 99 %), rubidium iodide (RbI, 99.9%), rubidium carbonate ($Rb_2CO_3$, 99.9%), 4-terc-butylpyridine (tBP; 98%), Lithium bis(trifluoromethanesulfonyl)imide (LiTFSI; 99.95 %), and anhydrous solvents (dimethyl formamide – DMF, dimethyl sulfoxide – DMSO, ethanol – EtOH, acetonitrile – ACN, and chlorobenzene) were purchased from Sigma-Aldrich, São Paulo, Brazil. Isopropanol (IPA, 99.9%) was purchased from Synth, Brazil–SP. Formamidinium iodide (FAI) and FTO coated glasses (TEC7) were supplied by GreatCell Solar LTD, Queanbeyan, Australia.

### Synthesis of the rubidium butyrate (RbBu)

Rubidium carbonate ($Rb_2CO_3$; 1 mmol; 231 mg) was added slowly in 2 mL of butyric acid ($BuCO_2H$; 21.8 mmol; 1.92 mg) under constant stirring, and the resulting solution was heated at T = 100 ºC until completion of the gas evolution. After cooling the solution, 10 mL of diethyl ether ($Et_2O$) was added in order to precipitate the rubidium butyrate (RbBu). The resulting solid was centrifuged, washed two times with 10 mL of $Et_2O$, dried under reduced pressure and stored at a dry and inert atmosphere.

### Preparation of Perovskite and Surface Modification with RbBu

The mixed halide perovskite solution was obtained from the equivalent proportional weight of each precursor in the same glass flask, considering 9% excess of $PbI_2$: CsI = 51.9 mg; FAI = 309.5 mg; $PbI_2$ = 686.9 mg; and $PbBr_2$ = 187.2 mg. Finally, 2 mL of DMF:DMSO (4:1) was added and the resulting solution of $Cs_{0.10}FA_{0.90}Pb(I_{0.83}Br_{0.17})_3$ was stirred overnight. The CsFAMA solution was prepared by a precursor solution containing FAI (1 M), $PbI_2$ (1.1

M), MABr (0.2 M), $PbBr_2$ (0.2 M) in anhydrous DMF:DMSO 4:1 (v:v): This composition contains excess of 9 % of $PbI_2$. 5% of volume of CsI 1.5 M stock solution in DMSO was added to previous perovskite solution.

The perovskite thin-films were obtained from two-steps, spin-coating deposition method. Firstly, 50 μL of the perovskite solution was added in a clean glass subtract, and it started to spin at 1000 rpm (2000 rpm $s^{-1}$) for 10 s. The substrate was accelerated to 4000 rpm (2000 rpm $s^{-1}$) for 30 s. At the final 10 s, 200 μL of the antisolvent (chlorobenzene) was added to the perovskite, forming a transparent-brown thin-film that was annealed in a hot-plate at 100 ºC for 30 min in a nitrogen-filled glovebox.

After the annealing, the thin-films were cooled to room temperature. The surface modification of the perovskite was done by single-step using 150 μL of the RbBu solution (1, 5, 10, 50 and 100 mM in IPA – dried using 4 Å molecular sieves) in a similar way to the antisolvent deposition (4000 rpm in the last 10s). The resulting modified perovskite thin-films were annealed at 100 ºC for 5 minutes in a nitrogen-filled glovebox.

**Structural Characterizations**

The SEM images were obtained on a Thermo Fisher Scientific Quanta™ 250 FEG-SEM at 10 kV, under high vacuum ($1.24x10^{-4}$ Pa), magnitude of $10^5$x and with an Everhart-Thornley Detector (ETD). NMR-MAS spectra were collected in a Bruker Avance II+ 400 MHz (9.4 T) spectrometer, with $^{1}H$ frequency of 400.13 MHz, $^{13}C$ frequency of 100.61 MHz and $^{87}Rb$ frequency of 130.92 MHz. The proton decoupled $^{87}Rb$ MAS spectrum was acquired with a $\pi/20$ pulse, calibrated to solid rubidium iodine, resulting in a pulse length of 0.217 μs. The MAS spin rate was 15 kHz. Due to the small amount of rubidium in the sample, an interval between acquisitions of 2 s was used. For reference, TMS was used for $^{13}C$ and $^{1}H$, and for $^{87}Rb$ aqueous rubidium chloride was used. $^{87}Rb$ spectrum for the 100 mM RbBu

modified LHP sample 241,276 scans were acquired, resulting in approximately 5.6 days of acquisition time. For the solid RbI precursor 128 scans were acquired, and for the RbBu 1,816 scans were acquired. $^{13}C$ spectrum with cross-polarization was obtained with a $\pi/2$ pulse length of 2.5 μs in the $^{1}H$, a contact time of 3 ms, and 1 s between acquisitions. MAS spin rate was 10 kHz. The number of acquisitions for the 10-RbBu sample was 2,357 scans. $^{1}H$ spectrum was obtained with a $\mu/2$ pulse length of 3.461 μs in the $^{1}H$ and 1 s between acquisitions. MAS spin rate was 15 kHz. The number of acquisitions for the 100 mM RbBu sample was 8 scans. Grazing Incidence Wide Angle X-ray Scattering (GIWAXS) measurements were performed at XRD2 beamline at the Brazilian Synchrotron Light Laboratory (LNLS) with X-ray energy of 7 keV, using the Pilatus 300K detector with 3 seconds of integration time. The incidence angle of the X-ray beam relative to the film surface was set at 3°. Each GIWAXS image was azimuthally integrated to obtain 1D X-ray diffraction patterns using pyFAI python libraries. The intensity was normalized by the storage ring current. X-ray Photoelectron Spectra (XPS) were acquired under a pressure of $10^{-9}$ Pa with a Scient Omicron ESCA+ spectrometer with a high-performance hemispheric analyzer (EA-125). The excitation source used was a monochromatic Al Kα (1486.6 eV) beam. The data was analyzed in CasaXPS, setting the C 1s peak at 284.8 eV as the reference for calibration.

## Optical Characterization

Electronic absorption spectra of the perovskite thin-films and its modifications were acquired with a *Hewlett-Packard* 8452A diode array spectrophotometer. Steady-state photoluminescence (PL) spectra were recorded in an OceanOptics 2000+ USB spectrometer, using a Kimmon He:Cd CW laser ($\lambda_{exc}$ = 442 nm; power = 300 W). The emission ranges

were recorded from 288 nm to 1039 nm. The films were oriented in a front-face configuration at 22.5º in order to minimize the Rayleigh light scattering of the excitation source.

## Charge Carrier Dynamics and Mobility Measurements

The charge carrier dynamics of the pristine and its RbBu modified LHPs were recorded using time-correlated single-photon counting (TCSPC) in a Edinburg Analytical Instruments FL 900 spectrofluorometer with an MCP-PMT (Hamamatsu R3809U-50; 50 ps) with a PicoQuant LDH-D-C-440 pulsed diode laser operating at $\lambda_{exc}$ = 440 nm (bandwidth of 5 nm, pulsewidth = 80 ps; F = 9.7 nJ $cm^{-2}$). The decay signals were collected at the maxima emission wavelength of each sample in a time scale of 2 μs. The instrument response was recorded using a Ludox sample.

Optical-Pump THz-Probe (OPTP) measurements were performed using a Spectra Physics Mai Tai-Ascend-Spitfire Pro Ti:Sapphire regenerative amplifier generating 35 fs pulses at a repetition rate of 5 kHz. The optical pump excitation was obtained by frequency doubling the 800 nm laser output through a BBO crystal, resulting in 400 nm pulses. THz probe pulses were generated by a spintronic emitter which was composed of 1:8nm of $Co_{40}Fe_{40}B_{20}$ sandwiched between 2 nm of Tungsten and 2 nm of Platinum, all supported by a quartz substrate. Detection of the THz pulses was performed using electro-optic sampling in a ZnTe crystal (0.2 mm (110)-ZnTe on 3 mm (100)-ZnTe). The sample, THz emitter and THz detector were held under vacuum ($<10^{-2}$ mbar) during the measurements. OPTP measurements reveal no fluence dependence of the charge-carrier mobilities in each sample, for variation of the fluence of the laser from 0.9 to 32.2 μJ $cm^{-2}$ (Figure S7 and S8), which indicates negligible contribution from nonlinear processes during the measurements at these experimental conditions. The effective mobilities were extracted from the differential

transmission of the THz probe immediately after t = 0 according to the method previously reported in Wehrenfennig et al., Adv. Mater. 2014, 26, 1584.[1]

**Perovskite Solar Cells (PSCs) Assemble**

FTO-coated glass substrates were cleaned using Hellmanex solution (2% v/v in water) with a toothbrush. Sequentially, substrates were placed in an ultrasonic bath with Hellmanex solution for 30 min, washed with deionized water (Milli-Q®) and EtOH. Finally, they were sonicated with IPA for 15 min, rinsed with acetone, and dried with compress air. Further $O_3$(g) plasma treatment was carried out for 10 min. The $SnO_2$ planar layer was deposited by spin-coating technique (3000 rpm; 200 rpm $s^{-1}$) using an IPA solution of pentahydrate tin(IV) chloride ($SnCl_4.5H_2O$; 0.05 mol $L^{-1}$). They were placed in a hotplate (T = 100 $^oC$), heated to 180 $^oC$ for 1h, and then treated with ozone plasma once again. Then, the substrates were placed in a Glovebox filled with nitrogen and were used for deposition of the perovskite layer. The perovskite films were deposited using the solvent engineering method.[35] Following a two steps procedure: 10 s at 1000 rpm (200 rpm $s^{-1}$) and 30 s at 4000 rpm (2000 rpm $s^{-1}$). The antisolvent was dripped onto the spinning substrate 15 s left to stop. The surface modifications were made in the same way that thin-films for optical and structural characterization. Then, the films were annealed at 100 $^oC$ for 30 min. The hole transport material (HTM) was prepared by dissolution of 2,2',7,7'-tetrakis(N,N'-di-p-methoxyphenyl-amine)- 9,9'-spirobifluorene (spiro-OMeTAD), lithium bis(tri-fluoromethanesulfonyl)imide (Li-TFSI, 1.8M in acetonitrile) , tert-butylpyridine (tBP) and tris(2-(1H-pyrazol-1-yl)-4-tert-butylpyridine)cobalt(III)tri[bis(trifluoromethane)sulfonimide] (FK209, 0.25M in acetonitrile) in the proportion 1:3.3:0.5:0.05 in chlorobenzene. The HTM solution was spin coated dynamically on a rotating substrate at 4000 rpm. An 80 nm-thick gold top electrode was deposited as a top contact electrode by thermal evaporation under high vacuum.

**Photovoltaic performance measurements**

The solar cells were measured using a 450 W xenon light source (Oriel). The light intensity was calibrated with a Si photodiode equipped with an IR-cutoff filter (KG3, Schott) and it was recorded during each measurement. The current-voltage characteristics of the cells were obtained by applying an external voltage bias while measuring the current response with a digital source meter (Keithley 2400). The voltage scan rate was 10 mV $s^{-1}$ and no device preconditioning were applied before starting the measurement. The cells were masked with a black meta mask limiting the active area to 0.158 $cm^2$ and reducing the influence of the scattered light. The photocurrent density was scaled to 1000 W $m^{-2}$.

Stability test of the solar cells was carried out under a full AM 1.5 Sun-equivalent white LED lamp and $N_2$(g) flow. The device area was masked to around 0.16 cm2. The devices were measured at MPP tracking under continuous illumination. The MPP was updated every 10 s. Every 15 min. a J-V curve was recorded.

**Theoretical Calculations**

Geometry optimization and electrostatic surface of $Bu^-$ anion were performed under the DFT framework using density-functional B3LYP[2], using a triple-zeta Pople's basis-set with polarization and diffuse functions (6-311++G**)[3–5] level. Calculations were done using the ORCA 4.2.1[6] and Avogadro[7] visualization software.

**Additional Characterization Data**

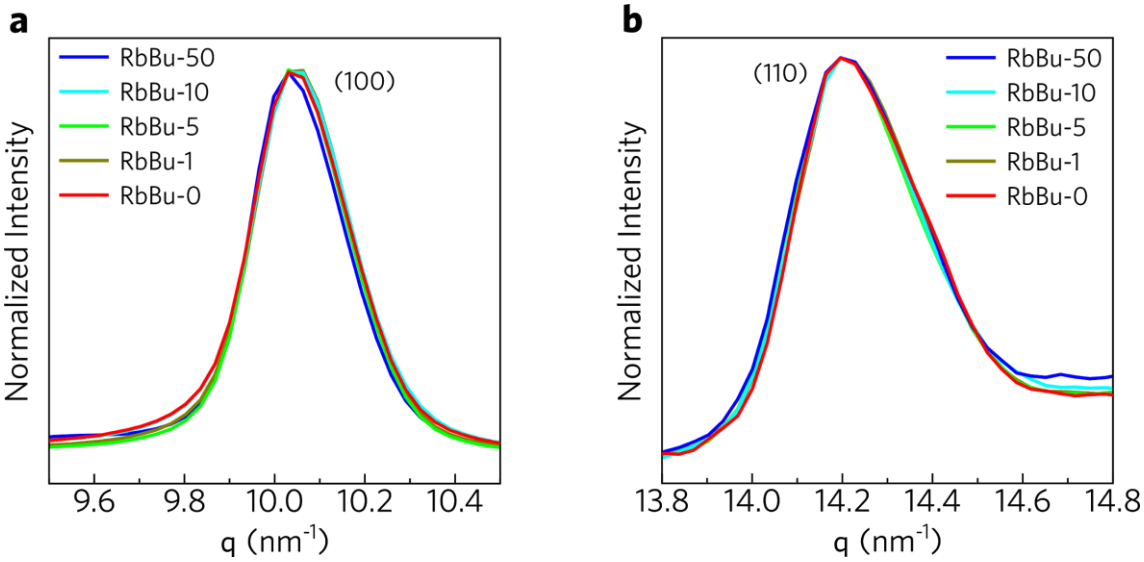


**Figure S1**. Zoom into the (a) (100) and (c) (110) peaks of the XRD patterns.

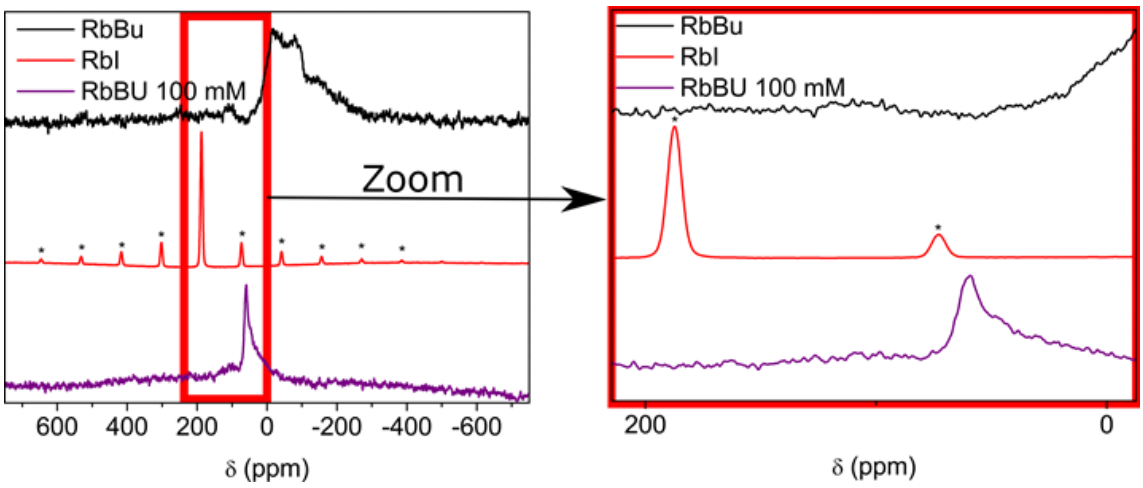


**Figure S2.** $^{87}$Rb-MAS-NMR spectra of RbBu (black), RbI (red) and RbBu-100 (purple).

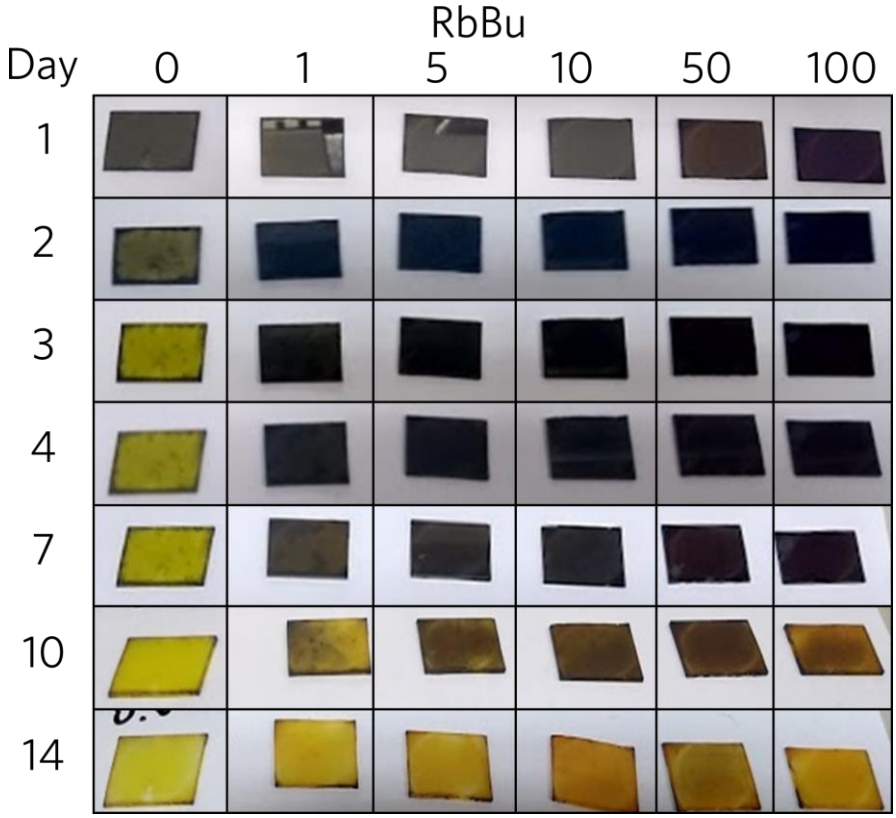


**Figure S3:** Visual stability test of CsFA perovskite deposited onto glass and exposed to air with relative humidity of 40-60% for two weeks.

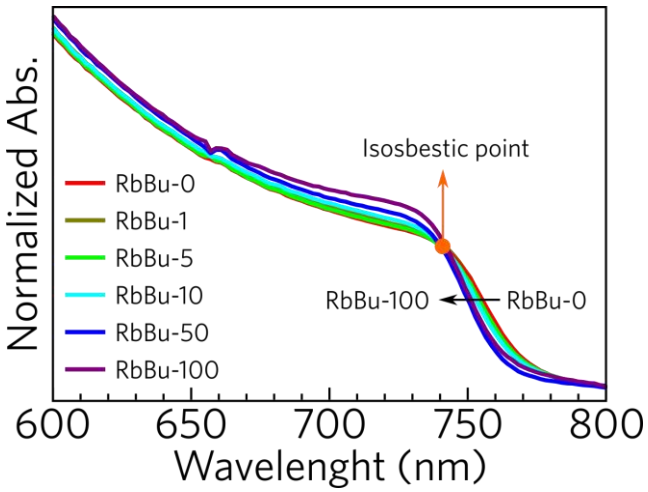


**Figure S4:** UV-Vis absorption spectra of the perovskite films passivated with RbBu.

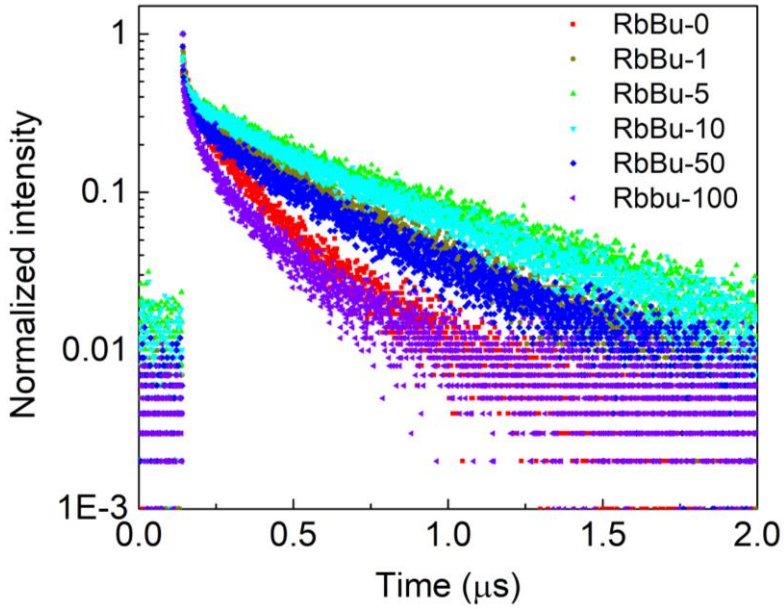


**Figure S5**. TRPL decays of pristine and surface modified samples by RbBu solutions ($\lambda_{exc}$ = 440 nm; $\lambda_{PL}$ = 760 nm; F = 9.7 nJ $cm^{-2}$).

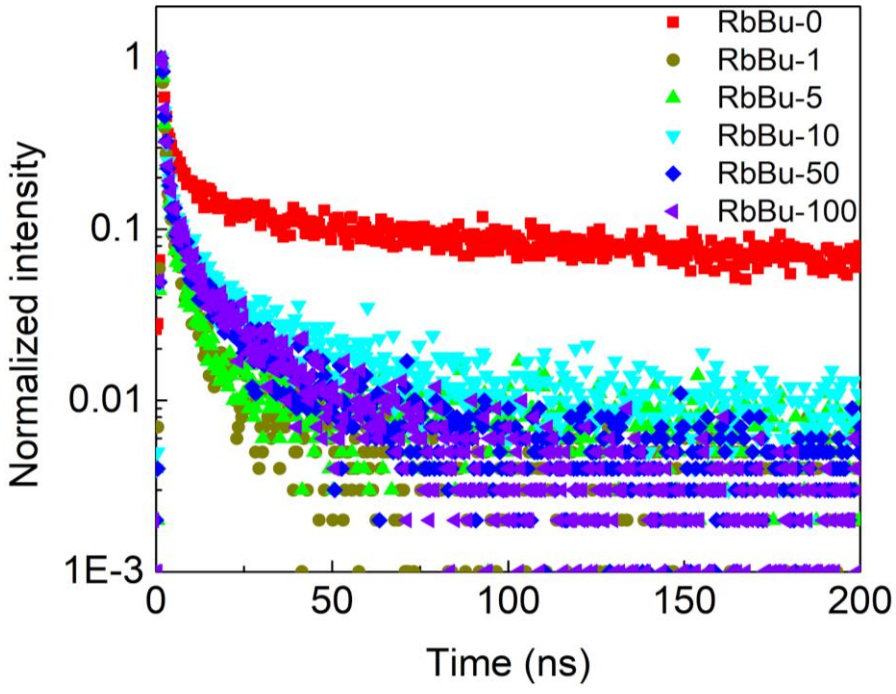


**Figure S6**. TRPL decays of pristine and surface modified samples by RbBu solutions with Spiro-OMeTAD layer on the top of the films ($\lambda_{exc}$ = 440 nm; $\lambda_{PL}$ = 760 nm; F = 9.7 nJ $cm^{-2}$).

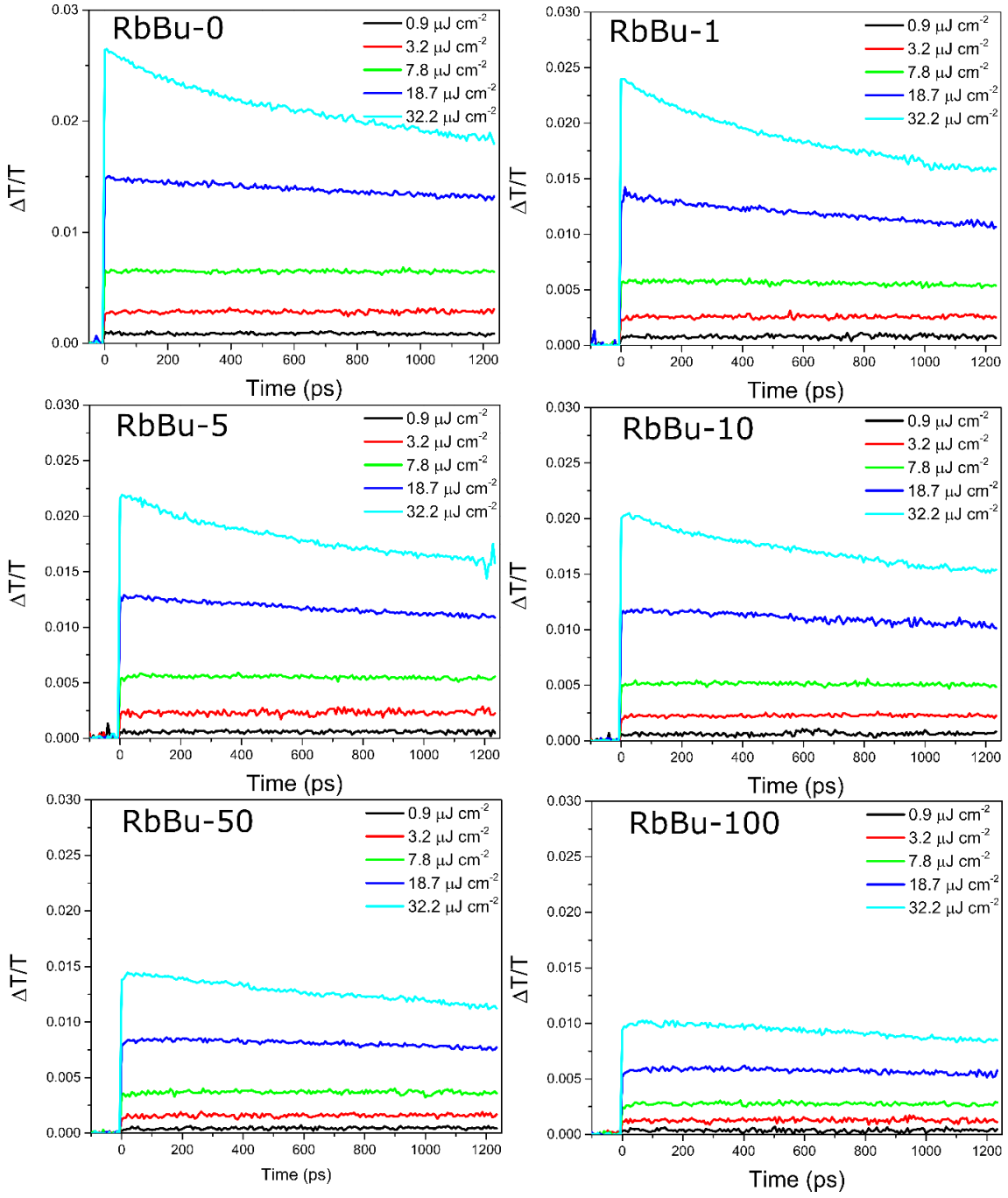


**Figure S7**. OPTP decays varying the laser fluence for the pristine and surface modified films with RbBu post passivation additive ($\lambda_{pump}$ = 400 nm).

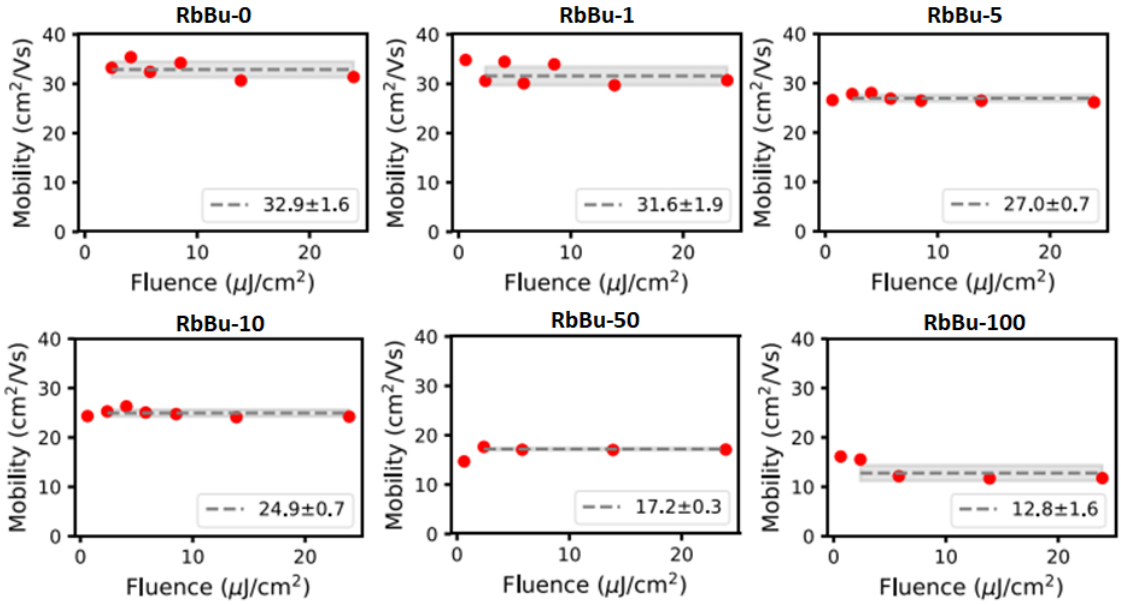


**Figure S8**. THz charge-carrier mobilities as function of the laser fluence for the pristine and surface modified films with RbBu post passivation additive.

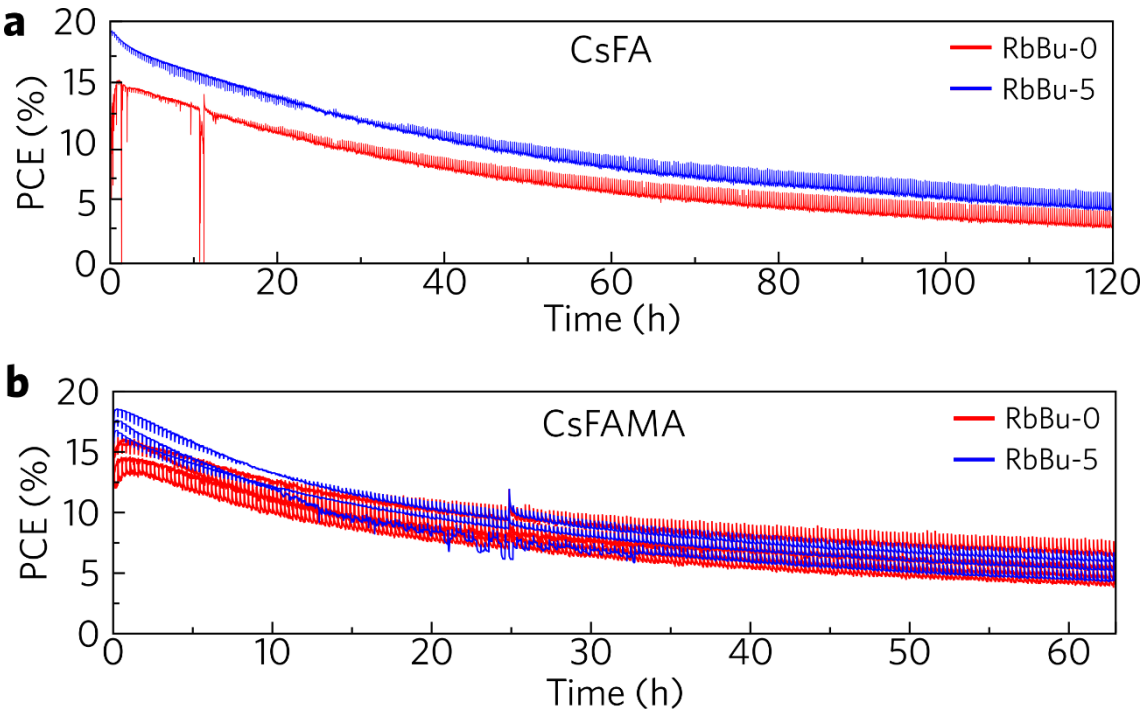


**Figure S9**: PCE obtained at MPP aging in inert atmosphere ($N_2$) and under 1 sun continuous illumination of PSCs with and without RbBu passivation for (a) CsFA and (b) CsFAMA perovskites.

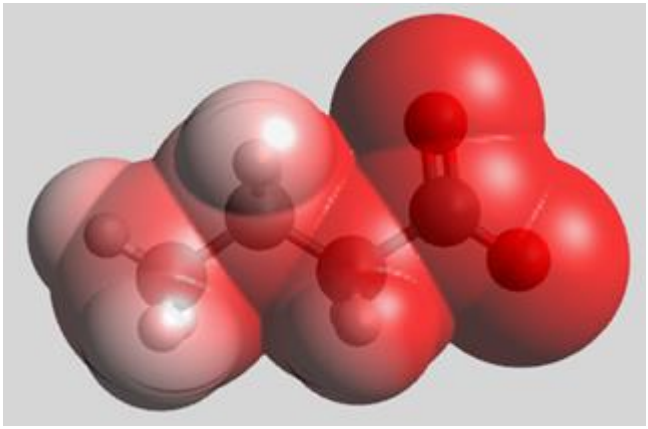

**Figure S10**: Optimized geometry and electrostatic surface volume of $Bu^-$ anion. Increment of red color indicates the negative charge distribution along the molecule.

**Table S1.** Resume of the charge-carrier lifetimes ($\tau_S$), $\beta_S$, first-order rates ($k_1$) (from TRPL), mobilities (from OPTP) measured at front ($\mu_F$) and back ($\mu_B$) face orientations, and charge-carrier diffusion lengths ($L_D$) for the post treated perovskites with RbBu solutions.

| **RbBu** (mM) | $\tau_S$ (ns) | $\beta_S$ | $k_1$ ($s^{-1}$) | $R^2$ | $\mu_F$ ($cm^2\ V^{-1}\ s^{-1}$) | $\mu_B$ ($cm^2\ V^{-1}\ s^{-1}$) | $L_D$ (μm) |
|---|---|---|---|---|---|---|---|
| **0** | 168 | 1 | $5.95x10^6$ | 0.963 | 31.9 | 39.1 | 3.69 |
| **1** | 185 | 0.706 | $3.82x10^6$ | 0.949 | 30.3 | 37.0 | 4.49 |
| **5** | 210 | 0.574 | $2.73x10^6$ | 0.962 | 26.8 | 36.5 | 5.00 |
| **10** | 199 | 0.589 | $2.96x10^6$ | 0.961 | 24.7 | 37.0 | 4.61 |
| **50** | 142 | 0.636 | $4.48x10^6$ | 0.942 | 17.2 | 35.7 | 3.13 |
| **100** | 134 | 1 | $7.46x10^6$ | 0.883 | 12.9 | 33.4 | 2.10 |

**Table S2.** Resume of the PSCs parameters.

| | | $V_{oc}$ (V) | $J_{SC}$ (mA cm$^{-2}$) | FF | PCE (%) | MPP (%) |
|---|---|---|---|---|---|---|
| **RbBu-0** | **F** | 1.10±0.01 | 22.1±0.2 | 0.64±0.02 | 15.5±0.7 | 13.9±1.8 |
| | **B** | 1.14±0.02 | 22.0±0.2 | 0.67±0.03 | 16.9±0.8 | |
| **RbBu-1** | **F** | 1.14±0.01 | 22.2±0.1 | 0.68±0.01 | 17.3±0.2 | 16.8±0.6 |
| | **B** | 1.16±0.01 | 22.1±0.2 | 0.69±0.01 | 17.7±0.2 | |
| **RbBu-5** | **F** | 1.14±0.01 | 22.0±0.1 | 0.71±0.01 | 17.7±0.2 | 17.2±0.2 |
| | **B** | 1.15±0.01 | 22.0±0.2 | 0.69±0.01 | 17.6±0.3 | |
| **RbBu-10** | **F** | 1.12±0.01 | 22.3±0.1 | 0.65±0.02 | 16.1±0.8 | 15.5±1.1 |
| | **B** | 1.15±0.01 | 22.1±0.2 | 0.67±0.01 | 17.0±0.5 | |
| **RbBu-50** | **F** | 1.14±0.01 | 22.0±0.2 | 0.65±0.02 | 16.5±0.6 | 15.9±0.3 |
| | **B** | 1.17±0.01 | 21.9±0.2 | 0.68±0.02 | 17.3±0.6 | |
| **RbBu-100** | **F** | 1.09±0.02 | 21.8±0.1 | 0.59±0.03 | 14.0±0.9 | 12.6±1.3 |
| | **B** | 1.11±0.03 | 21.4±0.4 | 0.61±0.04 | 14.5±1.5 | |

**Supporting Text 1**

We performed solid-state magic-angle nuclear magnetic resonance (MAS-NMR) of $^{87}$Rb (Figures S2). These experiments were done only for the most concentrated sample (RbBu-100). In the $^{87}$Rb-MAS-NMR spectra, a clear $^{87}$Rb resonance peak at $\delta$ = 63 and 59 ppm is observed, most likely related to the $\delta$-$RbPb(Br_xI_{1-x})_3$ non-perovskite phases, with a similar spectral shape in comparison with a previous work published by Kubicki *et al.* 2017.[8] A discreet large signal at 46 ppm is probably related to the presence of $Rb^+$ cations passivating the surface defects of A-site or interstitial sites on the surface of LHP grains. Also, no formation of the RbI ($\delta$ = 187 and 73 ppm) and RbBr ($\delta$ = 150 ppm),[8] or vestiges of RbBu (large resonance at $\delta$ < 0 ppm, due to its amorphous nature; see Figure S2), can be observed in the $^{87}$Rb-MAS-NMR spectra.

**Supporting Text 2**

The total charge-carrier recombination dynamics in LHPs can be obtained by a third-order rate equation:

$$\frac{dn(t)}{dt} = -k_3 n^3 - k_2 n^2 - k_1 n \quad \text{(S1)}$$

where $n$ is the charge-carrier density, $t$ is the time, $k_1$ is the first-order (monomolecular trap-assisted), $k_2$ is the second-order (bimolecular band-to-band), and $k_3$ is the third-order (Auger) recombination rates, respectively. The contribution of the high-order charge-carrier dynamics can be neglected in a time-correlated single photon counting (TCSPC) experiment at low-fluence regimes (F = 9.7 nJ $cm^{-2}$).[9] The monoexponential decay common function does not adjust the TRPL decays due to the disorder and aleatorily of the perovskites films and processing conditions.[10] Therefore, a stretched exponential decay function were used in order to extract the charge-carrier lifetimes, using the following equation:

$$I(t) = I_0 e^{-(\frac{t}{\tau_S})^{\beta_S}} \quad \text{(S2)}$$

where $I$(t) is the time-dependent intensity, $I_0$ is the intensity at the "zero" time, $\tau_S$ is the charge-carrier lifetime, and $\beta_S$ is the stretching factor, which varies between $0.5 < \beta_S \leq 1$ and is directly related to the LHPs thin-film disorder. As a consequence of the stretched exponential model, the first-order recombination rate is expressed by equation 3:[11,12]

$$k_1 = \frac{\beta_S}{\tau_S}(\frac{t}{\tau_S})^{\beta_S - 1} \quad \text{(S3)}$$

**Supporting text 3**

In order to verify in more details, the chemical composition on the perovskite surface after passivation, we carried out X-Ray photoelectron spectroscopy (XPS). Figure S11 displays the Rb 3d XPS for RbBu and perovskites. The perovskite film without RbBu does not show any Rb 3d peak, as expected, and the same for samples RbBu-1 and RbBu-5 due to small amounts of Rb. For sample RbBu-10 small peaks from Rb 3d ($3d_{3/2}$ = 111.5 eV and $3d_{5/2}$ = 109.9 eV) were detected. We attributed these peaks to $Rb^+$ passivating halide defects located near grain boundaries. For RbBu-50 and RbBu-100 new peaks at higher energy (112.2 and 110.8 eV) emerged. These new peaks are attributed to δ-$RbPb(Br_xI_{1-x})_3$ formed by the higher amount of $Rb^+$ introduced by the passivation consistent with XRD pattern.

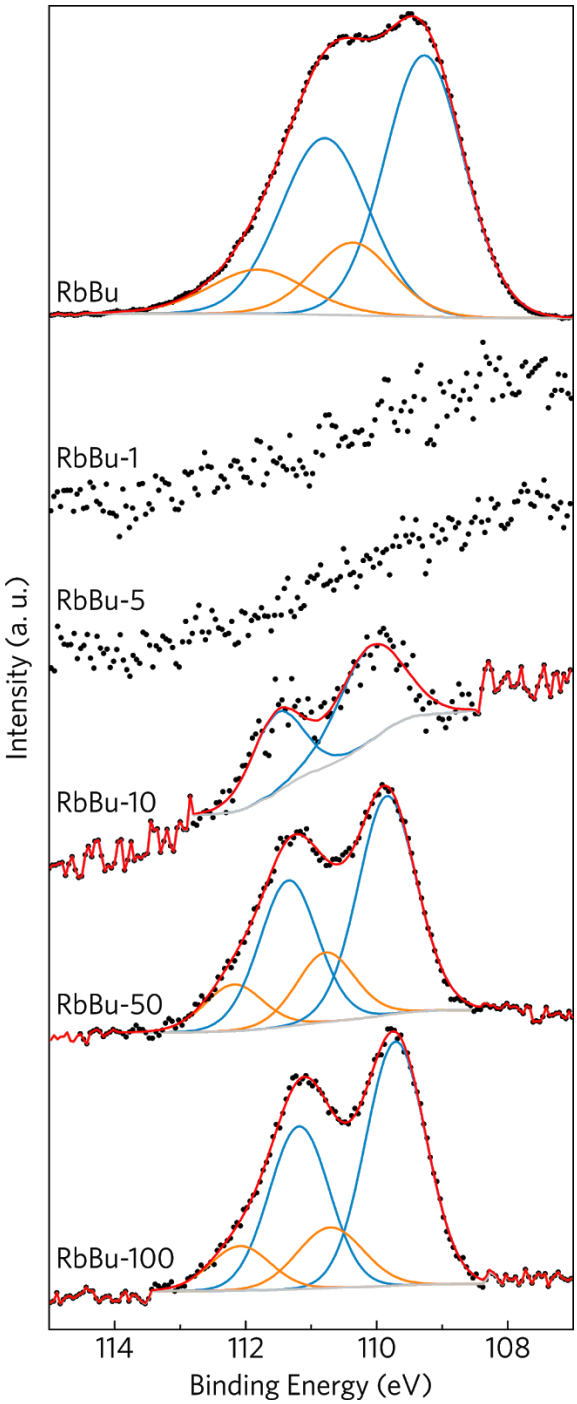


**Figure S11:** High resolution XPS spectra for RbBu and perovskite films with passivation.

## References

(1) Wehrenfennig, C.; Eperon, G. E.; Johnston, M. B.; Snaith, H. J.; Herz, L. M. High Charge Carrier Mobilities and Lifetimes in Organolead Trihalide Perovskites. *Adv. Mater.* **2014**, *26* (10), 1584–1589.

(2) Becke, A. D. Density-Functional Thermochemistry. III. The Role of Exact Exchange. *J. Chem. Phys.* **1993**, *98* (7), 5648–5652.

(3) Krishnan, R.; Binkley, J. S.; Seeger, R.; Pople, J. A. Self-Consistent Molecular Orbital Methods. XX. A Basis Set for Correlated Wave Functions. *J. Chem. Phys.* **1980**, *72* (1), 650–654.

(4) Clark, T.; Chandrasekhar, J.; Spitznagel, G. W.; Schleyer, P. V. R. Efficient Diffuse Function-augmented Basis Sets for Anion Calculations. III. The 3-21+G Basis Set for First-row Elements, Li–F. *J. Comput. Chem.* **1983**, *4* (3), 294–301.

(5) Frisch, M. J.; Pople, J. A.; Binkley, J. S. Self-Consistent Molecular Orbital Methods 25. Supplementary Functions for Gaussian Basis Sets. *J. Chem. Phys.* **1984**, *80* (7), 3265–3269.

(6) Neese, F. Software Update: The ORCA Program System, Version 4.0. *Wiley Interdiscip. Rev. Comput. Mol. Sci.* **2018**, *8* (1), 1–6.

(7) Hanwell, M. D.; Curtis, D. E.; Lonie, D. C.; Vandermeersch, T.; Zurek, E.; Hutchison, G. R. Avogadro: An Advanced Semantic Chemical Editor, Visualization, and Analysis Platform. *Adv. Math. (N. Y).* **2012**, 4–17.

(8) Kubicki, D. J.; Prochowicz, D.; Hofstetter, A.; Zakeeruddin, S. M.; Grätzel, M.; Emsley, L. Phase Segregation in Cs-, Rb- and K-Doped Mixed-Cation (MA)x(FA)1–XPbI3 Hybrid Perovskites from Solid-State NMR. *J. Am. Chem. Soc.* **2017**, *139* (40), 14173–14180.

(9) Johnston, M. B.; Herz, L. M. Hybrid Perovskites for Photovoltaics: Charge-Carrier Recombination, Diffusion, and Radiative Efficiencies. *Acc. Chem. Res.* **2016**, *49* (1), 146–154.

(10) Dequilettes, D. W.; Frohna, K.; Emin, D.; Kirchartz, T.; Bulovic, V.; Ginger, D. S.; Stranks, S. D. Charge-Carrier Recombination in Halide Perovskites. *Chem. Rev.* **2019**,

*119* (20), 11007–11019.

(11) Berberan-Santos, M. N.; Bodunov, E. N.; Valeur, B. Mathematical Functions for the Analysis of Luminescence Decays with Underlying Distributions 1. Kohlrausch Decay Function (Stretched Exponential). *Chem. Phys.* **2005**, *315* (1–2), 171–182.

(12) Stranks, S. D.; Eperon, G. E.; Grancini, G.; Menelaou, C.; Alcocer, M. J. P.; Leijtens, T.; Herz, L. M.; Petrozza, A.; Snaith, H. J. Electron-Hole Diffusion Lengths Exceeding Trihalide Perovskite Absorber. *Science (80-. ).* **2013**, *342* (October), 341–344.